A Large Excess in Apparent Solar Oblateness Due to Surface Magnetism

Martin D. Fivian, *et al.*

Science **322**, 560 (2008);
DOI: 10.1126/science.1160863

11. S. T. Fletcher, W. J. Chaplin, Y. Elsworth, J. Schou, D. Buzasi, in *Proceedings SOHO 18/GONG 2006/HELAS I, Beyond the Spherical Sun*, K. Fletcher, M. Thompson, Eds. (ESA SP-624, ESA Publications Division, Noordwijk, Netherlands, 2006), published on CDROM, p. 27.1.
12. J. W. Harvey, *Proceedings Future Missions in Solar, Heliospheric and Space Plasma Physics*, E. Rolfe, B. Battrick, Eds. (ESA-SP 235, ESA Publications Division, Noordwijk, Netherlands, 1985), pp. 199-208.
13. The large separation (Δ) refers to the first order regular spacing in frequency between consecutive overtone eigenfrequencies, responsible for the characteristic comb-like pattern of the oscillation spectrum.
14. H. Kjeldsen *et al.*, *Astrophys. J.* **635**, 1281 (2005).
15. Materials and methods are available as supporting material on *Science* Online.
16. C. Frohlich *et al.*, *Sol. Phys.* **170**, 1 (1997).
17. R. Samadi *et al.*, *Astron. Astrophys.* **463**, 297 (2007).
18. H. Kjeldsen, T. R. Bedding, *Astron. Astrophys.* **293**, 87 (1995).
19. F. Baudin, R. Samadi, T. Appourchaux, E. Michel, in *The CoRoT Mission, Pre-Launch Status, Stellar Seismology and Planet Finding*, M. Fridlund, A. Baglin, J. Lochard, L. Conroy, Eds. (ESA SP-1306, ESA Publications Division, Noordwijk, Netherlands, 2006), pp. 403–407.
20. Y. Lebreton, E. Michel, *Astrophys. Space Sci.* **316**, 167 (2008).
21. The CoRoT space mission, launched on December 2006, was developed and is operated by CNES (Centre National d'Etudes Spatiales), with participation of the Science Program of ESA, ESA's RSSD (Research and Scientific Support Department), Austria, Belgium, Brazil, Germany, and Spain. We acknowledge the access to data from the VIRGO instrument aboard SOHO, the mission of international collaboration between ESA and NASA.

Supporting Online Material

www.sciencemag.org/cgi/content/full/322/5901/558/DC1
SOM Text
Fig. S1
Table S1
References

9 July 2008; accepted 10 September 2008
10.1126/science.1163004

A Large Excess in Apparent Solar Oblateness Due to Surface Magnetism

Martin D. Fivian,[1]* Hugh S. Hudson,[1] Robert P. Lin,[1,2] H. Jabran Zahid[1,3]

The shape of the Sun subtly reflects its rotation and internal flows. The surface rotation rate, ~2 kilometers per second at the equator, predicts an oblateness (equator-pole radius difference) of 7.8 milli–arc seconds, or ~0.001%. Observations from the Reuven Ramaty High-Energy Solar Spectroscopic Imager satellite show unexpectedly large flattening, relative to the expectation from surface rotation. This excess is dominated by the quadrupole term and gives a total oblateness of 10.77 ± 0.44 milli–arc seconds. The position of the limb correlates with a sensitive extreme ultraviolet proxy, the 284 angstrom limb brightness. We relate the larger radius values to magnetic elements in the enhanced network and use the correlation to correct for it as a systematic error term in the oblateness measurement. The corrected oblateness of the nonmagnetic Sun is 8.01 ± 0.14 milli–arc seconds, which is near the value expected from rotation.

Motions within the interior of the Sun affect the location of the photosphere, so the precise measurement of the shape of the solar limb is a long-standing astrometric objective (*1*). The shape also relates to Le Verrier's 1859 observation of an anomalous perihelion precession of Mercury (only some 43″ per century), which could be precisely calculated in Einstein's theory of general relativity (*2*). A discrepancy from the predictions of this theory would point to either a need for a new theory or else to a distortion of the Sun's internal gravity not reflected in the surface rotation. The two leading possibilities for such a gravitational field would be a rapidly rotating core left over from the early stages of star formation—perhaps on an oblique axis—or a strong magnetic field (*3*).

The modern era of measurements of the solar oblateness began in the 1960s with Dicke's Princeton Solar Distortion Telescope (*4*) and other ground-based telescopes (*5*–*8*). Dicke's initial results (*4*) implied that the Sun was much more oblate than the surface rotation predicts. More recent observations have tended to show smaller values, closer to the 7.8 milli–arc sec predicted by the surface rotation (*3*), but the uncertainties in the measurements have remained relatively large. The theoretical estimate is difficult because of the differential nature of solar rotation, both in latitude and in radius. The ground-based data also hinted at time variations in the oblateness (*6*). Including the two data points (1997 and 2001) from the Michelson-Doppler Imager (*9*) on board the Solar Heliospheric Ob-

[1]Space Sciences Laboratory, University of California–Berkeley, Berkeley, CA 94720, USA. [2]Physics Department, University of California–Berkeley, Berkeley, CA 94720, USA. [3]Institute for Astronomy, University of Hawaii, Manoa, HI 96822, USA.

*To whom correspondence should be addressed. E-mail: mfivian@ssl.berkeley.edu

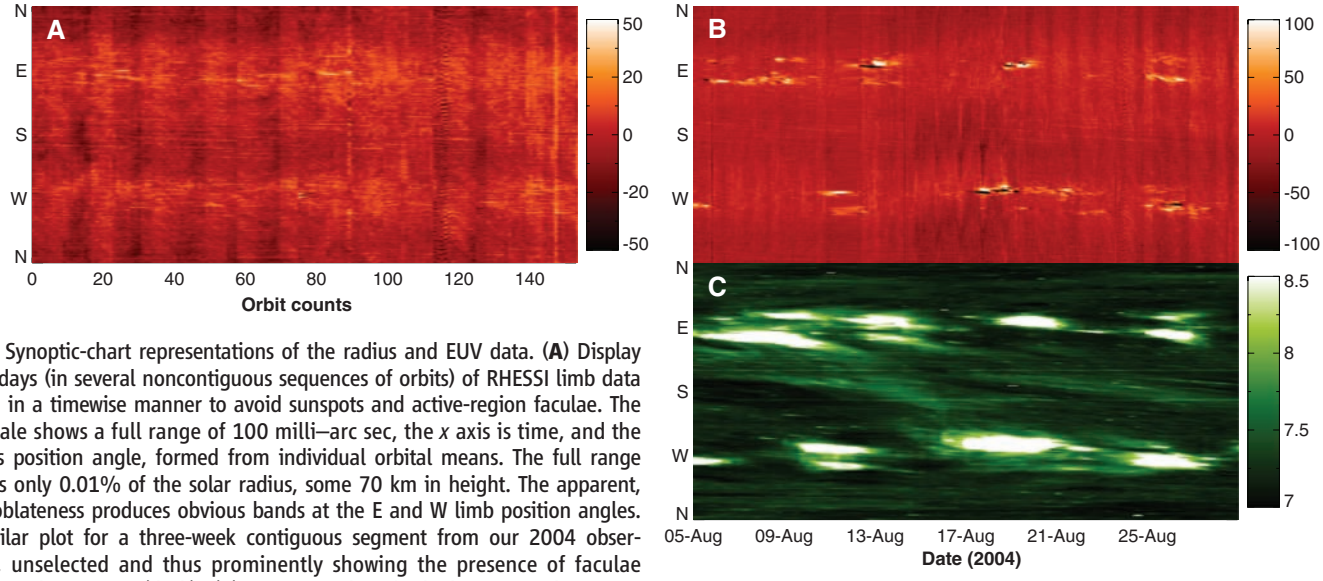

Fig. 1. Synoptic-chart representations of the radius and EUV data. (**A**) Display of ~10 days (in several noncontiguous sequences of orbits) of RHESSI limb data selected in a timewise manner to avoid sunspots and active-region faculae. The color scale shows a full range of 100 milli–arc sec, the *x* axis is time, and the *y* axis is position angle, formed from individual orbital means. The full range shown is only 0.01% of the solar radius, some 70 km in height. The apparent, excess oblateness produces obvious bands at the E and W limb position angles. (**B**) Similar plot for a three-week contiguous segment from our 2004 observations, unselected and thus prominently showing the presence of faculae (bright) and sunspots (dark). (**C**) Corresponding limb data from the SOHO observations in the EUV 284 Å band (*18*), which shows the locations of faculae and other kinds of magnetic activity. The contours of this synoptic map determine the data fraction for our masking analysis, as detailed in the SOM.

servatory (*10*) (SOHO/MDI), the first measurements from a satellite (*11*, *12*) further hinted at a solar-cycle variation. The balloon (*13*) and satellite (*12*) instruments yielded uncertainties on the order of 1 milli–arc sec in the oblateness. We report an order-of-magnitude reduction of these uncertainties from the new Reuven Ramaty High-Energy Solar Spectroscopic Imager (RHESSI) observations.

RHESSI is a solar x-ray/γ-ray observatory, and our astrometric data come serendipitously from its solar aspect sensor (SAS) (*14*, *15*), as described in the supporting online material (SOM). The RHESSI measurement essentially follows Dicke's method of using a rapidly rotating telescope to control systematic errors. The SAS consists of three independent optical systems, each with a simple lens (4-cm diameter) mounted on the front tray of the RHESSI modulation collimators and a linear charge-coupled device (CCD) sensor mounted on the rear tray at a separation of 1.55 m. The 2048-element CCD pixels are 1.73 arc sec square, and the observing wavelength is a 12-nm bandpass at 670 nm. The telemetry provides frequent samples (~16 s^{-1}) of each of the six limb intercepts in nominal pointing conditions, as well as full CCD images at a slower cadence (~1 min^{-1}). Data collection began in early February 2002 and continues to the present time.

We determine solar oblateness (equator-to-pole radius difference) from the axisymmetric quadrupole term of the Fourier components of the limb position given by the RHESSI data. The radius measurements are numerous, telemetered at ~100 samples per second, and are distributed approximately uniformly in azimuth around the limb. For this analysis, we averaged the data in 1°-bins and organized them (Fig. 1) as a function of two variables: (i) position angle (0 to 360° azimuth) and (ii) time. Each vertical line of such a synoptic plot shows the radius data from one RHESSI orbit (orbital period of 96 min). The color scale shows only a limited range of departures from the ephemeris reference value. Sunspots (negative excursions) and active-region faculae (positive excursions) produce obvious effects.

The RHESSI observations are differential measurements of the radius based on a simple fixed-brightness threshold (see SOM). This necessarily results in cross talk between limb po-

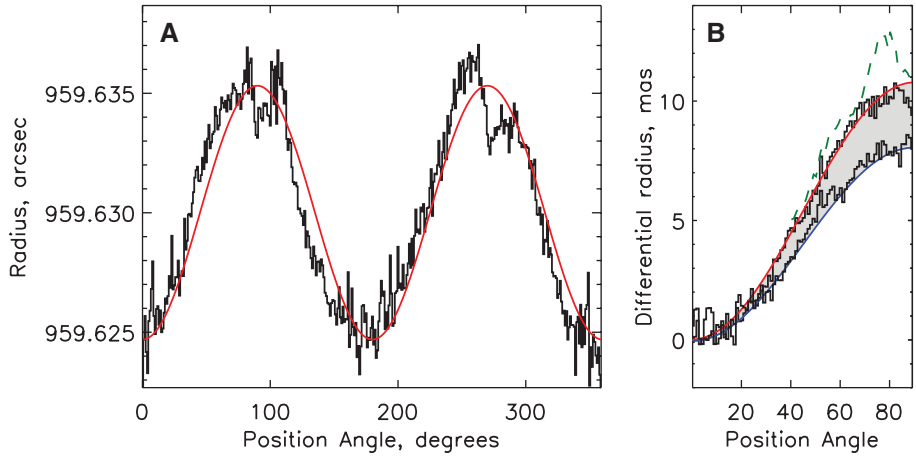

Fig. 2. Variation of apparent radius with position angle (azimuth). (**A**) Mean limb shape for the data set (Fig. 1) obtained from a timewise selection of visually clean orbits (i.e., those with minimal active-region faculae). The red line shows the fit of the axisymmetric quadrupole (l = 2) term showing an oblateness of 10.77 ± 0.44 milli–arc sec. Terms for the dipole and small (on the order of 1 milli–arc sec) hexadecapole have been subtracted from the data for clarity. Excesses near position angles 90 (W limb) and 270 (E limb) show the presence of some faculae, even in this "clean" data set. (**B**) Data folded onto one quadrant of position angle (colatitude). The red line shows the same fit as in (A), together with the overlaid data. The blue line shows a theoretical expectation (*3*). Masking against facular and faculalike confusion using the EIT data set (as shown in Fig. 1) results in a shape measurement with excellent agreement with this expectation (data over blue line). The dashed green line shows the whole unselected data set, including the strong facular signal but essentially having the same excess oblateness. mas, milli–arc sec.

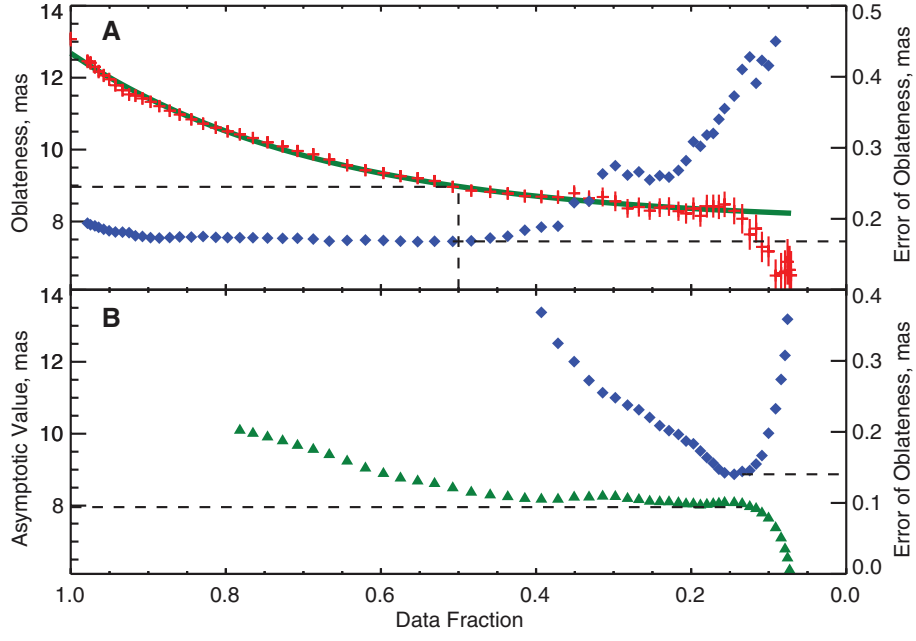

Fig. 3. Derivation of the oblateness measurement of the nonmagnetic Sun. (**A**) Oblateness fit (axisymmetric quadrupole term) as a function of the fraction of data incorporated in the analysis (red crosses), masking the RHESSI data against simultaneous EUV observations as described in the text. The blue diamonds show the orbit-to-orbit statistical errors (right y axis); i.e., the magnitudes of the error bars. The vertical dashed line shows the 50% point at which we are confident that the masking has removed faculae and little else. Because of the monotonic decrease of apparent oblateness versus data fraction, this point represents a conservative upper limit on the true oblateness. The horizontal dashed lines indicate its derived value and error of 8.96 ± 0.17 milli–arc sec. (**B**) Asymptotic value of oblateness (green triangles) from simple exponential model fit [green line in (A)]. The asymptotic values are derived by fitting the model up to and including the measurements of oblateness (red crosses) at the same data fraction. Including measurements of oblateness with smaller data fraction improves the determination of the asymptotic value (error from χ^2 minimization shown as blue diamonds, right y axis) down to a data fraction of 15%, but it is insensitive to the exact fraction beyond ~40%. The fit [green curve in (A)] and the asymptotic value of 8.01 ± 0.14 milli–arc sec for oblateness are derived by fitting measurements up to and including 15% data fraction, the minimum point of the χ^2 error fit.

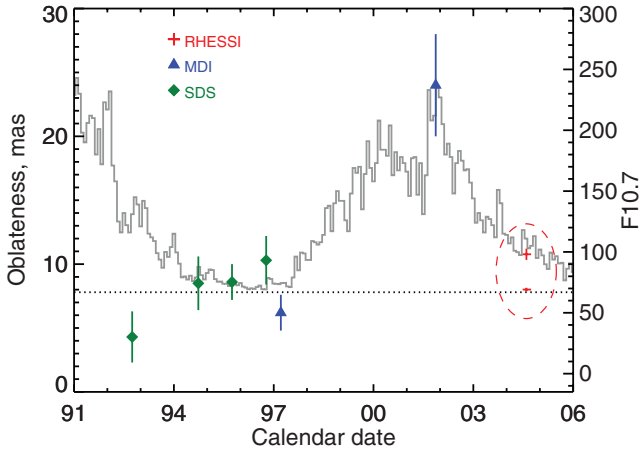

Fig. 4. Comparison of oblateness measurements from space. Here, we compare the RHESSI oblateness measurement, representing data from 29 June to 24 September 2004 (red crosses), with the best earlier values, namely the balloon-borne Solar Disk Sextant (SDS) experiment (green diamonds) (*13*) and the MDI instrument on board SOHO (blue triangles) (*12*). The surface rotation rate predicts the value shown with the dotted line. The histogram (scaled to the uniform-rotation oblateness at solar minimum and to the higher MDI data point) shows the radio flux index F10.7, a good indicator of the solar cycle. All errors are ±1σ.

sition and brightness (Fig. 1B) (*16*, *17*). Because of this cross talk, it is necessary to make a correction (prolate, 0.03 milli–arc sec) for ellipticity dimming as a result of Von Zeipel's theorem (*3*). We make the further strong assumption, discussed in detail in the SOM, that no other global brightness variation presently needs to be considered.

We averaged a synoptic map over time to produce a single shape profile (apparent radius versus position angle) for any particular set of orbits. A data set selected to avoid the obvious active-region faculae (synoptic plot shown in Fig. 1A) yields the limb profile of Fig. 2A. The oblateness (axisymmetric quadrupole) term dominates the shape and is 10.77 ± 0.44 milli–arc sec. This quantity is significantly (>6σ) larger than the prediction from surface rotation (*3*). Our 2004 result also differs significantly from either of the two SOHO/MDI results (*12*). The limb profile shows additional structure in higher-order Fourier components, but the bin-to-bin variation is relatively small.

In Fig. 2B, the red line shows the fit to a data set that does not include obvious active-region signatures. This selection still shows a large excess oblateness. Therefore, the analysis establishes that the active-region faculae do not solely produce the apparent excess oblateness. We need a new source spread around the surface of the Sun, and yet one that is concentrated into a predominantly axisymmetric quadrupole (apparent oblateness) component. Because of previous suggestions of a solar-cycle dependence, the sense of this discrepancy (an excess), and the appearance of the synoptic plots, processes related to solar magnetic activity are likely to be a direct cause.

We have made use of sensitive proxy data that show magnetic activity at the limb. The extreme ultraviolet (EUV) limb brightness (284 Å) from the EUV Imaging Telescope (*18*) on SOHO (SOHO/EIT) images correlates linearly with the RHESSI apparent radius (see SOM). We used this relation as a basis for data rejection to reduce the confusion with magnetic effects.

Corresponding to the threshold in the EUV data, the oblateness term decreases as more data are removed. Initially, there is a rapid decrease as the active regions are screened out and then a slower decrease as weaker faculalike regions are excluded. The oblateness as a function of data fraction inferred by this procedure has a plateau (Fig. 3A) and therefore gives us a robust measure of the oblateness in the absence of magnetic features. We also fit this monotonic decrease with an ad hoc exponential function (green line in Fig. 3) and take its asymptotic limit as a measure of the oblateness. We also find a stable limit for the asymptotic value as a function of data fraction and estimate its uncertainty by a weighted χ^2 minimization. The oblateness is 8.01 ± 0.14 milli–arc sec for a nonmagnetic Sun. This value is consistent within errors and model uncertainties of the prediction (*3*). The error estimate 0.14 milli–arc sec is smaller than those of previous observations. This error estimate (minimum of the diamonds in Fig. 3B) is consistent with the orbit-to-orbit scatter.

There are three distinct patterns in the limb profiles (Fig. 2B). The green dashed line shows the profile of the entire data set, and the active-region faculae appear prominently. If we reject the obvious faculae on an orbit-by-orbit basis (as shown in Fig. 1A), we obtain the data fit by the red line. This shows an excess oblateness, Δr, above that predicted by the surface rotation, Δr_{surf}, as described above. The blue line in Fig. 2B, based on our screening against EUV limb brightness, does not show the excess oblateness component and agrees with the oblateness expected from the surface rotation ($\Delta r_{surf} \approx 7.8$ milli–arc sec). We interpret the excess oblateness (red line) as the counterpart of the active network component of total irradiance variation (*19*, *20*), which is associated on a longer time scale with the redistribution of active-region magnetic flux to higher latitudes.

The oblateness measurements from space, prior to and including our RHESSI result, suggest variability (*6*, *12*), in spite of the large uncertainties (Fig. 4). Together the data also indicate an excess oblateness in the sense predicted by our identification of this phenomenon with the enhanced network. They also generally suggest a positive correlation with the solar cycle, again consistent with this notion. These appearances could also result from simple facular confusion (*16*), because the measurements from space may not have had adequate diagnostics for this systematic error. Our analysis of the EUV limb brightness points to the active network outside the faculae themselves as the source of this behavior.

The measured oblateness gives an estimate of the gravitational moment J2 via $J2 = (2/3)(\Delta r - \Delta r_{surf})/r_\odot$ (*6*), where Δr is our observed value of 8.01 ± 0.14 milli–arc sec, $\Delta r_{surf} \approx 7.8$ milli–arc sec (*3*), and $r_\odot$ denotes the mean solar radius, 95,963 arc sec. Formally, we obtain $J2 = (1.46 \pm 1.0) \times 10^{-7}$, a value consistent with other determinations (*21*, *22*). Here, the uncertainty does not include the uncertainty in the estimation of the rotational term.

References and Notes

1. A. Auwers, *Astron. Nachr.* **128**, 361 (1891).
2. C. M. Will, *Living Rev. Relativ.* **9**, 3 (2006).
3. R. H. Dicke, *Astrophys. J.* **159**, 1 (1970).
4. R. H. Dicke, H. M. Goldenberg, *Phys. Rev. Lett.* **18**, 313 (1967).
5. H. A. Hill *et al.*, *Phys. Rev. Lett.* **33**, 1497 (1974).
6. R. H. Dicke, J. R. Kuhn, K. G. Libbrecht, *Astrophys. J.* **318**, 451 (1987).
7. S. Sofia, W. Heaps, L. W. Twigg, *Astrophys. J.* **427**, 1048 (1994).
8. J. Rozelot, S. Lefebvre, V. Desnoux, *Sol. Phys.* **217**, 39 (2003).
9. P. H. Scherrer *et al.*, *Sol. Phys.* **162**, 129 (1995).
10. V. Domingo, B. Fleck, A. I. Poland, *Sol. Phys.* **162**, 1 (1995).
11. J. R. Kuhn, R. I. Bush, P. Scherrer, X. Scheick, *Nature* **392**, 155 (1998).
12. M. Emilio, R. I. Bush, J. Kuhn, P. Scherrer, *Astrophys. J.* **660**, L161 (2007).
13. A. Egidi *et al.*, *Sol. Phys.* **235**, 407 (2006).
14. M. Fivian, R. Henneck, A. Mchedlishvili, A. Zehnder, *Sol. Phys.* **210**, 87 (2002).
15. M. Fivian, R. Henneck, A. Zehnder, *Innovative Telescopes and Instrumentation for Solar Astrophysics*, S. L. Keil, S. V. Avakyan, Eds. (SPIE, Waikoloa, HI, 2003), vol. 4853, pp. 60–70.
16. G. A. Chapman, B. Ziegler, *Sol. Phys.* **168**, 259 (1996).
17. J. R. Kuhn, K. G. Libbrecht, R. H. Dicke, *Science* **242**, 908 (1988).
18. J.-P. Delaboudinière *et al.*, *Sol. Phys.* **162**, 291 (1995).
19. C. Zwaan, *Annu. Rev. Astron. Astrophys.* **25**, 83 (1987).
20. R. C. Willson, H. S. Hudson, *Nature* **351**, 42 (1991).
21. J. Armstrong, J. R. Kuhn, *Astrophys. J.* **525**, 533 (1999).
22. I. W. Roxburgh, *Astron. Astrophys.* **377**, 688 (2001).

23. We thank NASA for support under grants NAG5-12878 and NNX07A141G.

Supporting Online Material

www.sciencemag.org/cgi/content/full/1160863/DC1
SOM Text
Figs. S1 to S5
References

22 May 2008; accepted 24 September 2008
Published online 2 October 2008;
10.1126/science.1160863
Include this information when citing this paper.